Experimental study of the influence of the vents on the thermal performance of a Trombe wall

Afef LARIBI[1], Sylvie BEGOT*[1], Dominique SURDYK[1], Yacine AIT-OUMEZIANE[1], Valérie LEPILLER[1], Philippe DESEVAUX[1], Nour EL ZEIN[1], Ana RIBEIRO DE CARVALHO[1]

[1]Université de Franche-Comté, CNRS, institut FEMTO-ST, F-90000 Belfort, France
*(corresponding author: sylvie.begot@univ-fcomte.fr)

Keywords: Trombe wall, passive solar heating, thermal performance, vents

Highlights:

- Experimental study of a Trombe wall made of cellular concrete and its adjacent room
- Laboratory study conducted under conditions typical of the intermediate season.
- Influence of vent size and configuration on performance
- A substantial reduction in vent surface area is necessary to impact behavior.

Abstract

This article presents an experimental study of a Trombe wall made of cellular concrete, associated with different vent configurations. The experiments were conducted in the laboratory using a Trombe wall connected to an adjacent room, under conditions of an intermediate season. The measurements focus on temperature and heat flux measured in various areas of the facility. Five configurations are compared: one with the vents fully open, three with reduced vent surface areas and different positions, and one with the vents fully closed. The impact of the number and position of the vents on the thermal behavior and efficiency of the Trombe wall is measured and analyzed. The results indicate that only the configuration with the vents fully closed exhibits a very different thermal behavior compared to the other configurations. In this configuration, the insulating properties of cellular concrete result in a minimal temperature increase in the room, making it an appropriate solution for maintaining occupant comfort even during summer conditions. Configurations with partially closed vents show generally similar behavior, except when there are significant reductions in vent surface. To effectively limit convective transfer with partial vent closure, a substantial reduction in vent surface (at least 60%) is required.

Nomenclature

A	area, m²
D	distance of the top and bottom vents centers, m
f	decrement factor
g	acceleration of gravity, ms^{-2}
H	height of the wall, m
HF	heat flux sensor
c_p	specific heat capacity, $Jkg^{-1}K^{-1}$
C_d	discharge coefficient

$\dot{Q}$	heat transfer rate, W
$\dot{q}$	heat flux, Wm^{-2}
v	velocity, ms^{-1}
Ra	Rayleigh number
T	temperature, °C
T^{+}	dimensionless temperature
Tc	Thermocouple
TLL	Thermal Load Leveling
t	time, s
y	vertical coordinate, m
y^{+}	dimensionless vertical position

Greek

α	fluid thermal diffusivity, m^2s^{-1}
β	volumetric expansion coefficient, K^{-1}
η	efficiency
ε	emissivity
λ	thermal conductivity, $Wm^{-1}K^{-1}$
ν	fluid kinematic viscosity, m^2s^{-1}
ρ	density, kgm^{-3}

Subscripts

air	*air*
amb	ambient
b	bottom
Ch	channel
cond	conductive/conduction
conv	convective/convection
G	glass
in	inside
init	initial
mean	mean
out	outside
R	room
s	light source
sto	storage
t	top
V	vent
W	wall

1. Introduction

Buildings, as the most energy-intensive sector, account for 40% of final energy consumption in Europe [1]. A significant portion of this energy, primarily derived from fossil fuels, is used for heating and air conditioning to maintain comfortable living conditions. This reliance on fossil energy contributes to greenhouse gas emissions. Therefore, the adoption of renewable energy sources, such as solar energy, to reduce heating consumption through passive solar systems is of great importance [2], [3].

The Trombe wall is a construction solution invented and patented by American engineer Edward Sylvester Morse in 1881 [4]. It was called the Trombe Wall because it was first used by Felix Trombe and Jacques Michel (a French engineer and architect respectively) in a house in Odeillo, France, in 1967 [5].

Such a wall is a system composed, from the outside to the inside, of glazing separated from an opaque storage wall by an air channel. The thermal storage wall is dark-colored and constructed with materials of high thermal capacity in order to absorb solar radiation. The glass is used to transmit the light and create a greenhouse effect in the air channel. A space heating cycle is then created due to the air-density difference between the hot channel and the inside of the building [5]. In order to promote convective heat exchanges, vents are generally installed in the upper and lower parts of the storage wall. The integration of this wall into a building is done with the aim to recover as much solar energy as possible in order to heat the interior space in winter.

Numerous studies highlight the benefits of Trombe walls. For example, Jaber and Ajib [6] have numerically determined the optimal percentage of the Trombe wall surface in relation to the total surface area of the south-facing façade. The works of Kruger et al. [7] and Abdeen et al. [8] show that the integration of a Trombe wall into a room can save around 30% of heating energy and improve thermal comfort. Abassi et al. [9] have shown that a Trombe wall with a surface area of 8 m^2 allows an annual saving of heating energy of about 77% in a conventional home in Tunisia.

However, Trombe wall systems have certain disadvantages. In winter or at night, when sunlight is absent, a reverse recirculation phenomenon can occur, leading to heat loss to the outside. During the summer, these systems may also cause overheating. Several methods to enhance the thermal performance of Trombe wall systems have been explored and documented in the literature review conducted by Wang et al. [5]. Some of these works focus on the effect of the type of glazing [10], [11], [12], [13] or the addition of sun protection [14], [15], [16], [17], [18], [19].

When it comes to the study of the thermo-physical properties of the storage wall, it is well known that the construction material also plays a decisive role in the thermal performance of the wall. Regarding the use of materials to store sensible heat, Özbalta et al. [20] compared the performance of a concrete, brick or cellular concrete wall in cold climates, and have shown that cellular concrete allows an annual heat gain of between 4.3 and 13% depending on the color used. In 2012, Stazi et al. [21], carried out a parametric study to identify the influencing factors and subsequently optimize the performance of the Trombe wall. The results of this study showed that it is possible to reduce CO_2 emissions and energy consumption by up to 55% when the system consists of a solid, 20 cm thick cellular concrete wall and double glazing. Hu et al. [16], recommended the use of low-density materials because they minimize the energy consumption used to cool the room in summer. Briga Sá et al. [22], have analytically studied the effect of the materials making up the storage wall on the thermal gain achieved during the winter and summer periods. They showed that the use of bricks with a thickness equal to 40 cm offers very interesting thermal performance in terms of heating. Hernandez-Lopez et al. [23] tested different materials used in the solid wall such as concrete, brick and adobe. They showed that when the vents are opened, concrete can store 30% more than adobe and 23% more than brick. In 2019, Dong et al. [24] studied a newly designed cellular concrete Trombe wall where the absorber is a plate placed between the glass and the wall. They showed that the daily efficiency of their system was increased by 50%.

The study of vents and the control of their openings and closings is also a subject addressed by several authors. Warrington and Ameel [25] showed that heat transfer coefficients increased slightly as the mass transfer gaps in the Trombe wall were increased in size; however, increasing the gap sizes also caused an increased thermal stratification in the living space. Their work is experimental, using a 1/18th scale model with silicon oil as a convective fluid. Ben Yedder et al. [26] numerically showed that the air vent size and position have an influence on the energy transfer. Kurtbas et al. [27] have studied a Trombe wall with several vents. They showed in simulation that the average velocity of the air changes depending on the vent locations. While the average velocity of the air is maximum in the middle vents, it decreases away from the middle vents. Jaber et al. [6] modeled a Trombe wall where the vents are closed at night. Liu et al. [28] studied the optimal opening and closing times of the vents and showed that 2–3 hours opening after sunrise with closure 1 hour before sunset was optimal. He et al. [14] studied the control of the openings and closings of the vents in the case of a wall incorporating a Venetian blind. Briga Sá et al. [22] studied the cross-influence of ventilation and wall material.

The winter performance of Trombe walls has been extensively studied, but summer and intermediate season conditions have been studied less frequently. In 1997, Ghrab-Morcos et al. [29] studied solar passive buildings in Tunisia and showed that room temperature is highly stable, night ventilation plays an essential role in decreasing room temperature both at night and during daytime, Trombe wall screening is more efficient to canceling its solar gains than operating as a solar chimney. Performance indicators were internal temperature compared to ambient temperature and a comfort deviation factor. In 1998, Gan [30] studied the ventilation of Trombe wall for summer cooling with a CFD numerical analysis. It was found that the ventilation rate induced by the buoyancy effect increases with the wall temperature, solar heat gain, wall height, thickness and insulation, distance between wall and glazing. It was shown that in order to maximize the ventilation rate, the interior surface of a Trombe wall should be insulated for summer cooling. Performance indicators were air flow rate and wall temperature. Jaber and Ajib [6] recommended the use of roller shutters. Zalewski et al. [31] have shown that in a composite Trombe wall, the insulated panel plays its role in insulation during the summer. Torcellini and Pless [32] have shown that overhangs limit solar gain in summer except at the beginning and end of the day when the height of the sun is low. Performance indicators included Trombe wall temperature profiles, and thermographic images. Stazi et al. [33] have shown that the best performance for reducing cooling energy requirements in summer is achieved by combining overhangs, roller shutters and cross ventilation. Performance indicators were surface and air temperatures, and Predicted Mean Vote (PMV) comfort values. Simoes et al. [34] demonstrated through simulation that solar and Trombe walls can both lead to significant reductions in net energy demands if properly tailored shading devices and vents with specific seasonal and daily operation schedules are implemented. Performance indicators were temperature and energy demands. Bevilacqua et al. [35] demonstrated through simulation that a well-managed Trombe wall can be regarded as an interesting solution to achieve energy savings both in summer and winter. The implemented ventilation strategies allow for reducing electric demand for air-conditioning and, assuming proper management of the shading system and natural ventilation, cooling needs can be reduced by 9.5%. Performance indicators were temperature and energy demands.

To ensure the optimal performance of Trombe walls in all seasons, several areas still require investigation, particularly concerning vents. Additionally, there is a lack of experimental data for summer and intermediate season conditions. In this article, we focus on the experimental study of a Trombe wall made of cellular concrete, exploring specific vent configurations under intermediate season conditions. To the authors' knowledge, the configurations tested on the vents in this work have not been studied in the literature. In addition, to the authors' knowledge again, no study on Trombe walls made of aerated concrete includes a study on vents. Finally, the study fulfills a lack of experimental data on Trombe wall in intermediate seasons. Therefore, the paper presents experimental results from a Trombe wall constructed with cellular concrete, featuring various configurations and sizes of vents, along with their analysis. The experiments are conducted in a laboratory setting using a Trombe wall model connected to an adjacent room. Cellular concrete was selected due to its favorable performance regarding CO_2 emissions [21] and its insulating properties. We installed instrumentation, including thermocouples and heat flux sensors, to closely examine the thermal behavior of the system.

The first part of the article details the experimental design and analysis criteria, while the second part presents and discusses the results obtained.

2. Materials and Methods

2.1. Experimental setup

2.1.1. Geometric configuration of the Trombe wall and materials used

The experimental model represents a classic Trombe wall integrated with an adjacent room (Figure 1). The Trombe wall is composed, from the outside to the inside of a glazing separated from an opaque storage wall by a ventilated air space. In order to promote convective heat exchange, vents are installed in the upper and lower parts of the storage wall.

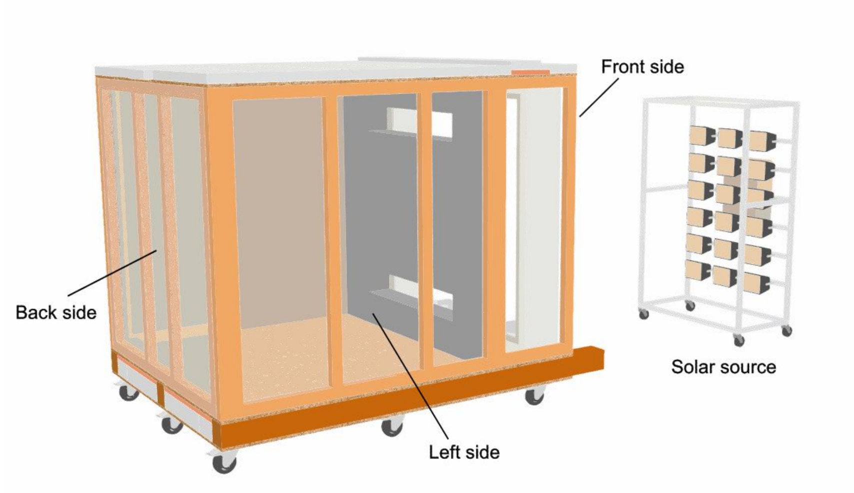

(a) 3D view of the model

(b) Trombe wall picture

Figure 1: Description of the different components of the Trombe wall

The facility is in the form of a parallelepiped 1.97 m high and 1.9 m wide (Figure 2). The glass wall is 8 mm thick and has a transparent surface area of 1.67x1.67 m^2. The air channel between the glass wall and the storage wall is 19 cm thick, which corresponds to a tenth of the height of the wall, a value usually recommended in the literature [5]. The vents at the top and bottom of the storage wall are rectangular (1.2 m long and 0.19 m high) and are spread almost across the entire width of the façade. The room to which the Trombe wall is connected is 1.97 x 1.9 x 1.8 m^3. The front side glass is supposed to be facing South, therefore the inside wall of the room at the opposite (backside) will be referred as the North wall.

The floor and ceiling are made of 18 mm thick OSB (Oriented Strand Board) panels, insulated from the outside by two layers of expanded and extruded polystyrene with thicknesses of 60 and 30 mm, respectively. The right, left and back walls are made of 6 mm thick wood fiber composite panels insulated from the outside with 60 mm thick expanded polystyrene.

The storage wall is made of 20 cm thick cellular concrete.

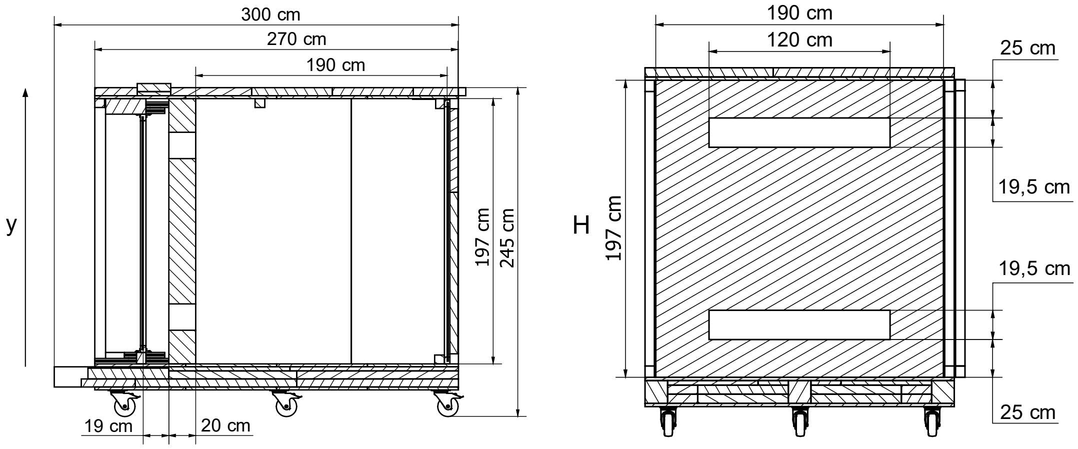

(a) (b)

Figure 2: Experimental setup dimensions: (a) Side section view, (b) Front section view

The thermo-physical properties of the materials used in the construction are presented in Table 1.

	ρ	c_P	λ	ε
Materials	kgm^{-3}	$Jkg^{-1}K^{-1}$	$Wm^{-1}K^{-1}$	-
Glass (Saint-Gobain Calumen III 1.18)	2500	800	1.02	0.89
Celullar concrete (Ytong Compact 20)	450	1000	0.11	0.85
Polystyrene (Prb-facade-Th38)	30	1450	0.038	0.9

Table 1: Thermo-physical properties of the materials used

2.1.2. Artificial light source

The solar irradiation of the wall is simulated using artificial lighting composed of 18 halogen projectors with 200W bulbs (Langlois SOL-COM 2). In order to ensure the homogeneity of the irradiation on the surface of the glass, the light source was placed 2.5 m from the wall.

2.1.3. Instrumentation

Temperature measurements are carried out in the air outside and inside the model as well as on certain surfaces. All temperature readings are provided by class I type K (chromel-alumel) thermocouples. The sensors used to measure conductive and radiative heat fluxes are the gradient heat flux sensors of Captec brand. Two types of sensors are used: conductive and radiative heat flux sensors. All sensors are connected to a National Instruments data acquisition system. The locations of the individual sensors are indicated in Figure 3, and their characteristics are listed in Table 2.

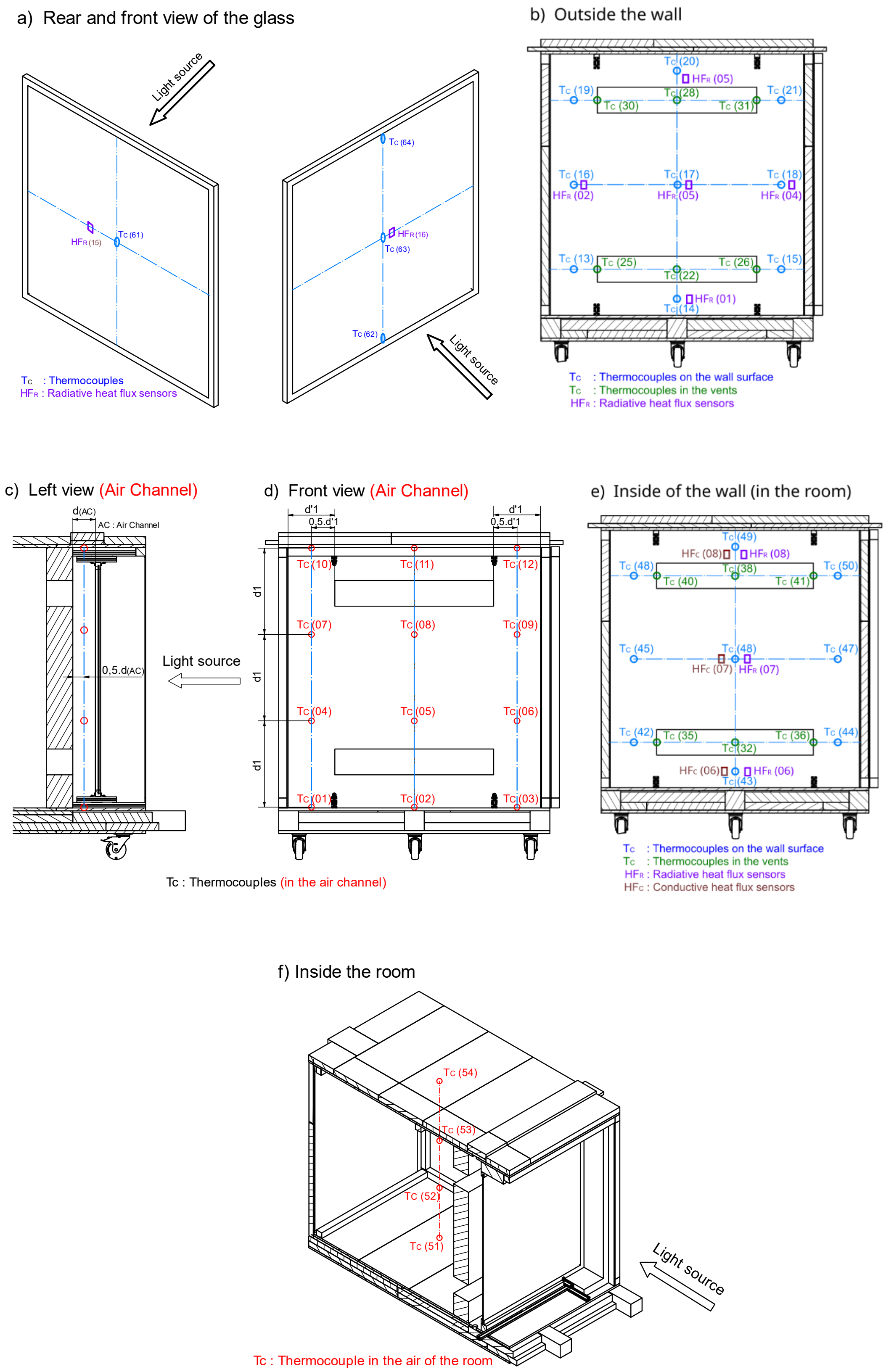

Figure 3: Location of the measurement sensors

Parameter	Unit	Sensor	Accuracy	Range
Temperature	°C	Thermocouple	±0,5	0 à 1100 °C
Irradiance	Wm^{-2}	Pyranometer	± 5 %	0 à 1500 Wm^{-2}
Heat flux	Wm^{-2}	Heat flux sensor	-	+/- 10 kWm^{-2}

Table 2: Characteristics of sensors

2.1.4. Vent configurations

The vents can be plugged with polystyrene blocks, which makes it possible to study different configurations. All the tested configurations are presented in Figure 4. The ratio between the sum of the surface area of the vents A_V and that of the wall is denoted A^+ with:

$$A^+ = \frac{2A_V}{A_W} \quad (1)$$

The basic configuration is as described above (2.1.1). In this configuration denoted C1, the vents have a height of 0.195 m and a width of 1.2 m, giving a value of 0.125 for A^+. For the C2 configuration, the height of the vents was halved across the entire width of the wall, resulting in a value for A^+ of 0.062. The C3 configuration is not uniform across the width of the wall. It has 2 open parts on either side of a closed part, giving a value A^+ of 0.083. In the C4 configuration, which is also not uniform, the width of the vent is reduced to 0.4 m, i.e. A^+ is 0.042. The C5 configuration corresponds to the case with the vents completely closed, A^+ is zero.

C1 - $A^+ = 0.125$	C2 - $A^+ = 0.062$	C3 - $A^+ = 0.083$ separated in 2	C4 - $A^+ = 0.042$	C5 - closed $A^+ = 0$

Figure 4: Vent configurations under study

2.2. Procedure and experimental protocol

The artificial light source was programmed to simulate the solar insolation for 5 hours (9 a.m. to 2:25 p.m.), with a sinusoidal flux peaking at 280 Wm^{-2} measured with the pyranometer on the outer surface of the glass. After the light source is switched off, the Trombe wall cools down freely. The total duration of the experiment is 24 hours. We denote this period as 360°, therefore the heating phase lasts 75°. The measured values are recorded in 5-minute intervals. The experimental setup is installed in a laboratory hall in which the temperature is around 18 °C.

2.3. Performance evaluation criteria

2.3.1. Notations and dimensionless numbers

The dimensionless height y^+ is calculated in relation to the total height of the wall H of 197 cm:

$$y^+ = \frac{y}{H} \tag{2}$$

The dimensionless temperature T^+ is calculated by the ratio between the temperature difference measured at the point under consideration with the ambient cold temperature and the temperature difference of the wall on the outside measured at $y^+ = 0.83$ with the ambient cold temperature T_{amb} [36]. The temperature measured on the outside wall at $y^+ = 0.83$ is chosen because it is the maximum temperature recorded in the experiment. T_{amb} is the coldest ambient temperature measured, therefore at the beginning of the experiment.

$$T^+ = \frac{T - T_{amb}}{T_{w,o,y+=0.83} - T_{amb}} \tag{3}$$

The Rayleigh number Ra_H is based on the height of the cavity i.e. H [31].

$$Ra_H = \frac{g\beta\left(T_{w,mean,o} - T_{Ch,mean}\right)H^3}{\nu\alpha} \tag{4}$$

2.3.2. Energy criteria

The performance of the system will be evaluated using energy efficiency η_{conv} , defined as the ratio between the energy transmitted to the room by convection through the vents and the energy received on the glass over a period of 24 hours [37], [38], [39]:

$$\eta_{conv} = \frac{\int_{24h} \dot{Q}_{conv} dt}{\int_{24h} \dot{Q}_s dt} \tag{5}$$

with $\dot{Q}_{conv}$ convective heat transfer rate transmitted to the room, $\dot{Q}_s$ power of the artificial light source received on the glazing. $\dot{Q}_{conv}$ is determined by measurements of the inlet and outlet temperatures of the vents, and the velocity which is evaluated using the correlation below [40]:

$$\dot{Q}_{conv} = \rho v_{air} A_V c_{P,air} (T_{V,t,mean} - T_{V,b,mean}) \tag{6}$$

$$v_{air} = C_d \sqrt{gD \frac{(T_{V,t,mean} - T_{V,b,mean})}{(T_{V,t,mean} + T_{V,b,mean})}} \tag{7}$$

with: $C_d = \sqrt{\frac{2}{\zeta}}$; $\zeta = C_1 \left(\frac{A_{Ch}}{A_V}\right)^2 + C_2$; $C_1 = 8$; $C_2 = 4$.

$T_{V,t,mean}$ and $T_{V,b,mean}$ are the mean temperatures respectively at the level of the top (t) and bottom (b) vent, v_{air} is the average air velocity, ρ is the density of the air at temperature T, c_p is the air specific heat capacity, C_d is the discharge coefficient, A_V and A_{Ch} are the passage sections of the vents and the channel respectively, g is the gravitational acceleration, D is the distance between the two vents.

A second criterion is that of the performance of the wall with regard to the heat storage in the solid wall. We define the criterion η_{sto} as the ratio between the maximum energy stored in the wall and the energy received on the glass over a period of one day:

$$\eta_{sto} = \frac{m_W c_{p,W} \Delta T_{W,mean,max}}{\int_{day} \dot{Q}_s dt} \quad (8)$$

$$\text{with } \Delta T_{W,mean,max} = T_{W,mean,max} - T_{W,mean,init} \quad (9)$$

This definition is therefore slightly different from that of Rabani et al. [41], who use the mean stored value.

2.3.3. Criteria linked to temperature

For the criteria related to temperature, a first criterion is the stability of the internal temperature of the room over time, Thermal Load Levelling, defined by [42]:

$$TLL = \frac{T_{R,max} - T_{R,min}}{T_{R,max} + T_{R,min}} \quad (10)$$

Thus, this criterion will be close to 0, when the temperature in the room is stable. This criterion therefore allows for assessing the capacity of the configuration to heat the room.

The second criterion concerns the attenuation of the temperature wave in the wall, a "decrement factor" f defined by [42]:

$$f = \frac{T_{W,in,max} - T_{W,in,min}}{T_{W,out,max} - T_{W,out,min}} \quad (11)$$

Thus, f will be equal to 1 if the same difference between the extreme temperatures is observed for the outer and inner sides of the wall, and closer to 0 if the temperature difference is attenuated. This criterion therefore allows for assessing the heat transfer between the exterior and interior side of the wall, which tends to homogenize the temperatures between both sides of the wall.

3. Results and discussion

First, we present in detail the two extreme cases of operation: configuration C1 where the passage section of the vents is the largest, and configuration C5 where the vents are closed. The evolution of the various sensor measurements over time is presented and analyzed. In a second part, we will make a comparative analysis of the five configurations, including those where the vents are partially open, based on the criteria defined above.

3.1. – Detailed study of extreme operating cases

3.1.1. Basic configuration C1: fully open vents

3.1.1.1. Measured quantities evolution with time

The Figure 7a presents the overall evolution of average temperatures in different areas of the test facility. First of all, we note that the ambient temperature is slightly variable and equal to an average of 18 °C. The temperature measured in the lower part of the device is lower, as the floor of the test room is poorly insulated.

The light source heat flux measured by the radiative heat flux sensor glued to the outside of the glass is also plotted on the graph. It reaches a maximum of 270 Wm^{-2}, consistent with the value of 277 Wm^{-2} measured at the same time by the pyranometer.

The average temperature at the external face of the black-painted solid wall is the highest, reaching a maximum value equal to about 38 °C, with a time lag of 1.8 hours (27°) compared to the maximum value of the light source heat flux. For this maximum wall temperature value, the Rayleigh number Ra_H is 6.5×10^8.

The temperature of the glass varies with a similar pace to that of the temperature of the outside side of the wall, the amplitude is slightly lower, with a maximum of 34°C on average. In descending order of maximum value, we observe the temperature of the glass on the inside of the channel, of the glass on the outside, in the channel, then the temperature in the room (maximum delayed of 2.6 h or 39°), and finally the temperature on the inside of the wall. This temperature variation has the largest delay (2.8 h or 42°) compared to the heat flux source due to the low conductivity of cellular concrete.

In Figure 7b and following, the temperatures at the different points of the test facility are plotted as a function of y^+ the dimensionless height. When several thermocouples are at the same height, the average value is presented. The temperature in the glass is uniform with a small difference between the inner and outer side (Figure 7b). The average temperature on the inside of the glass is 3°C higher than on the outside (Figure 7b). This is because the outer side of the glass exchanges with the surrounding air at room temperature of 18°C. The temperature at the bottom of the glass is lower due to the stratification of the ambient temperature and that of the channel.

In the channel (Figure 5c), we observe the stratification of the air, with an expected increase in temperature with height in the cavity. Four levels are instrumented as shown on Figure 3. The average maximum temperature is 29°C. This temperature distribution can also be observed on the surface temperatures of the wall, outside and inside (Figure 5d), the latter due to convective exchanges with the air. The delay between the maximum temperatures on the inside side and on the outside side is 1.5 hours (or 22.5°). At first, the temperature on the outside of the wall is higher than those on the inside. The temperature difference between the inside and outside of the wall is reversed 8 hours and 30 minutes (or 127.5°) after the start of the experiment, i.e. 5 hours (or 75°) after stopping the heat flux source.

Temperatures measured in the vents (Figure 5e) also show the temperature difference between the top and bottom of the room. The temperature difference between the upper and lower vents is at most 5°C, reflecting the overall temperature rise in the room. Finally, in the room (Figure 5f), the air temperature reaches 20°C in less than 2 hours (30°), except at ground level. It remains above 20°C for more than 6 hours (90°) after the light heat flux has stopped.

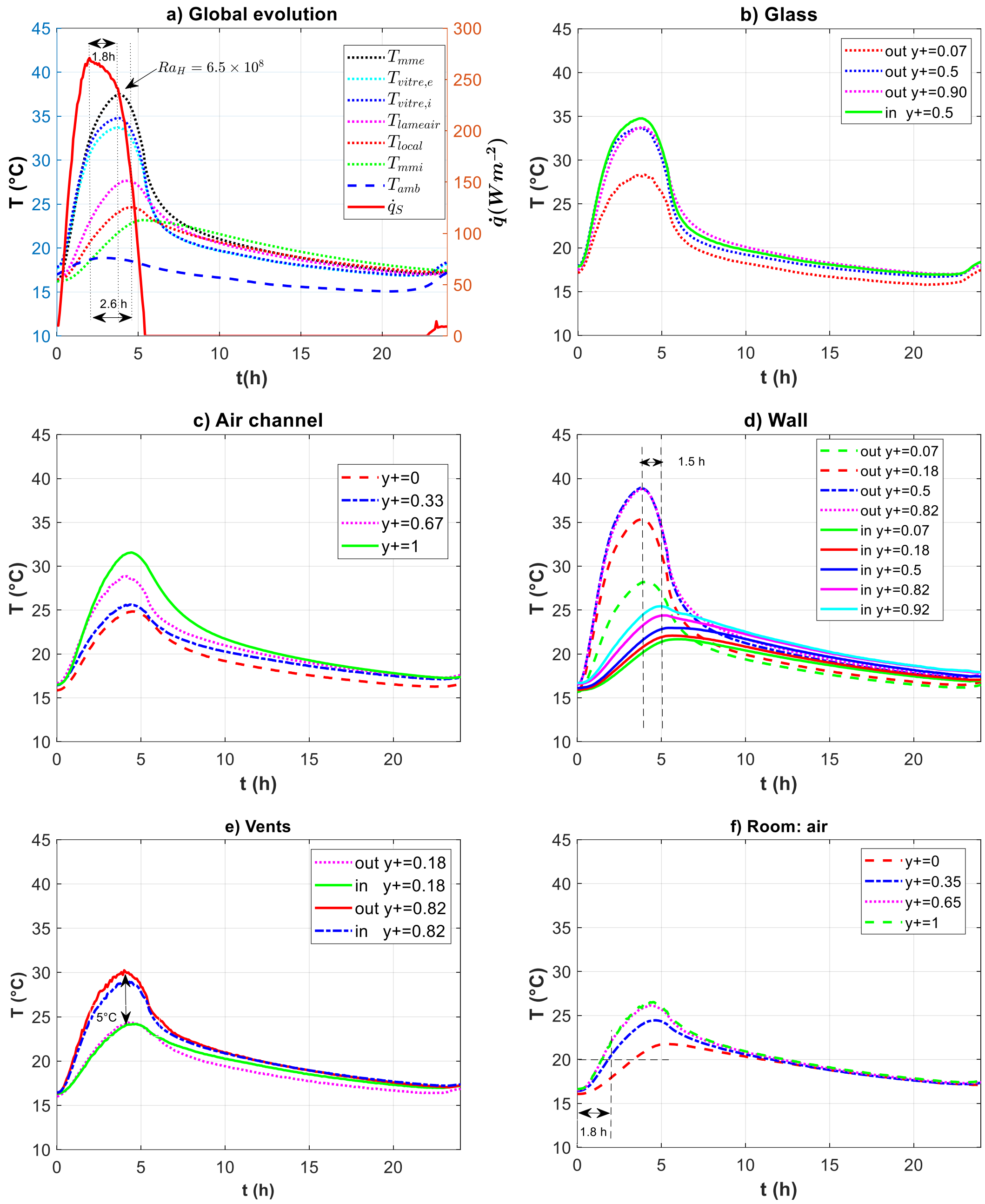

Figure 5: Configuration C1 $A^+ = 0.125$

The convective heat transfer rate, calculated using the equations (6) and (7), has a maximum value of 150 W (Figure 6a). This relatively low value is explained by the rapid rise in temperature in the room, which causes the difference between the temperatures of the upper and lower vents to be small. The volume of the adjacent room in the test facility is small. The delay between the maximum values of these heat fluxes is 1.3 hours (19.5°). The conductive heat flux density measured on average by the sensors placed on the surface of the solid wall has a negative value, meaning there is a heat flux from the inside of the room to the wall during the first hours of the experiment. This is due to the faster increase in the air temperature of the room compared to that of the interior surface of the wall as shown in Figure 6b. In this figure, we can see a strong correlation between this temperature difference and the heat flux density measured by the heat flux sensors. After 6 hours of experiment (90°), the temperature of the room becomes lower than that of the wall on the inside side, and the heat stored in the wall is transferred to the room. Therefore, the measured heat flux becomes positive. The heat exchange between the channel and the room is therefore mainly by thermo-circulation through the vents.

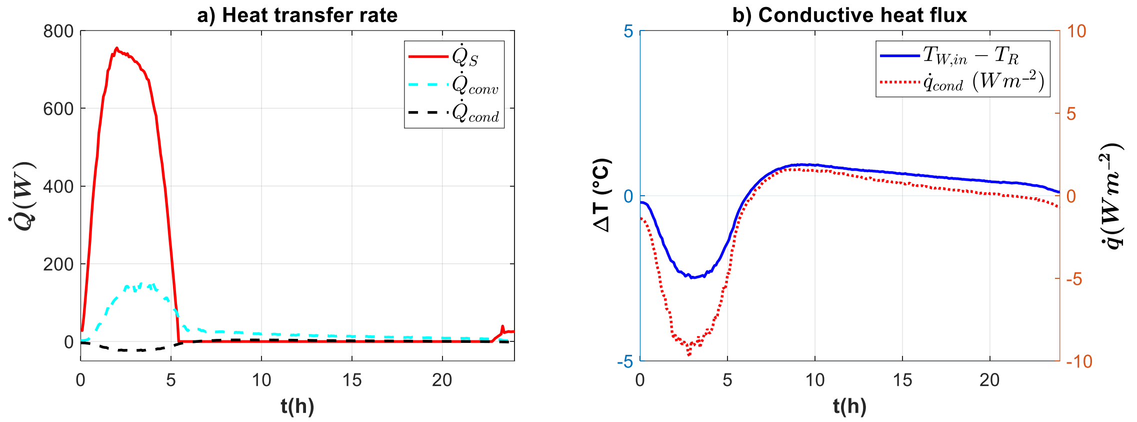

Figure 6: Configuration (C1) $A^{+} = 0.125$ *– Heat transfer*

3.1.2. Configuration closed vents C5

Figure 7a presents the overall evolution of the different quantities when the vents are fully closed. Closing the vents causes the room temperature to drop and its increase to slow down significantly. The maximum is reached after 9 hours (135°) instead of 2.6 hours (39°) in configuration C1 and the maximum temperature is less than 20°C, even in the upper part of the room (Figure 7f). Due to the stop of the convective flow through the vents, the temperatures of the channel increase significantly with a maximum of 35.5°C instead of 27.7°C when the vents are fully open (Figure 7c). As a result, the glass and outside wall temperatures are also increasing by about 5°C (Figure 7b and Figure 7d). Without convection, the phase shift between the temperature maximums on the inside and outside of the wall is clearly increasing. There is a difference of 5.75 h (86.3°) for a reduced height of 0.82 (Figure 7d).

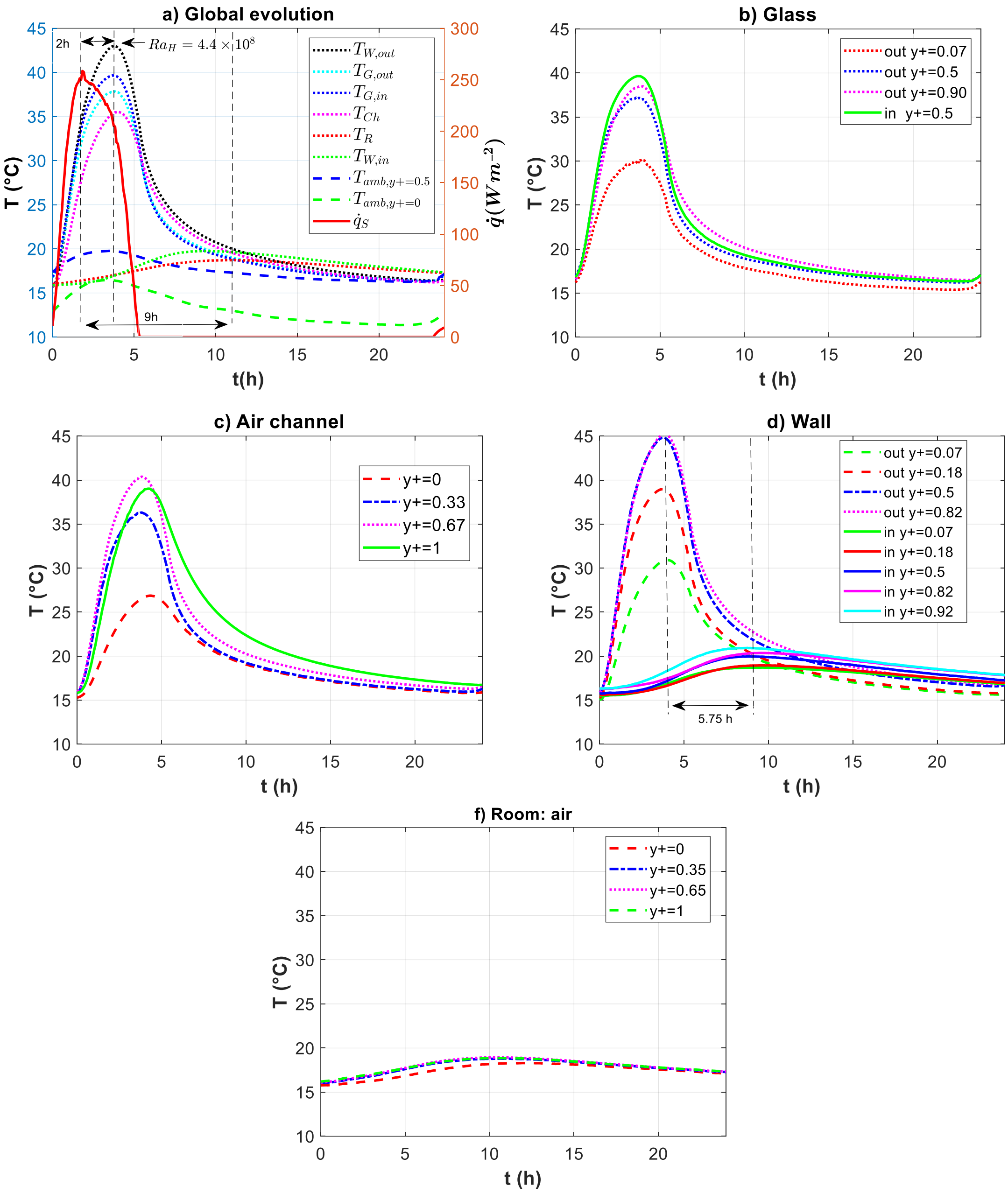

Figure 7: Configuration C5 $A^{+} = 0$ *– Temperature evolution*

The conductive heat transfer rate calculated from the measurements of heat flux sensors on the inside of the wall is significantly different from that measured in the previous case (Figure 8a). Indeed, since the temperature of the room is no longer influenced by the convective heat transfer rate through the vents, the temperature difference between the inside surface of the wall and the room quickly becomes positive (Figure 8a). However, the conductive flux density remains low, with a maximum value of less than 5 Wm^{-2}.

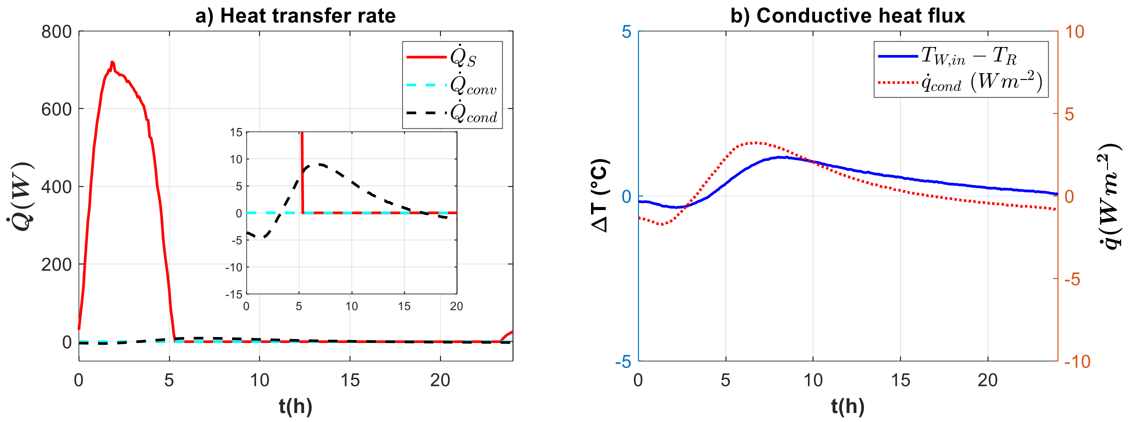

Figure 8: Configuration (C5)$A^+ = 0$ *– Heat transfer*

3.2. Influence of the vents on the behavior of the Trombe wall

After studying the extreme cases of operation (vents fully open, vents fully closed), we compare all the configurations with each other in the rest of this section.

3.2.1. Temperatures

Figure 9 shows the temperature rises for the different configurations. Overall, the temperature rises in configurations where the vents are open show fairly similar temperature rises compared to those observed in the case where the vents are closed.

The presence of an opening in the wall allows convective transfer to the room, which in any case leads to a lower temperature rise on the glass (Figure 9a), the outside wall (Figure 9c) and in the channel (Figure 9b).

On the inside of the wall (Figure 9d), when the vents are closed C5, the temperature depends only on the conductive heat transfer in the wall and is therefore delayed compared to that observed on the outside. In the case where the vents are open (C1 to C4), the inner wall exchanges by convection with the air coming from the vents and a faster rise is therefore observed.

The temperature difference between the high and low vents (Figure 9e) is relatively moderate with a maximum value of around 5°C. This is due to the small volume of the room.

In the room (Figure 9f), the temperature rise is very small, less than 3°C, if the vents are closed (C5). In all the cases where the vents are open, the elevation in the room is faster and higher. The C1 configuration, where the passage section is maximum leads to the greatest elevation, followed by the configuration C2 where the section is halved across the entire width of the wall. Configurations where openings are not distributed over the entire surface lead to a lower temperature rise in the room.

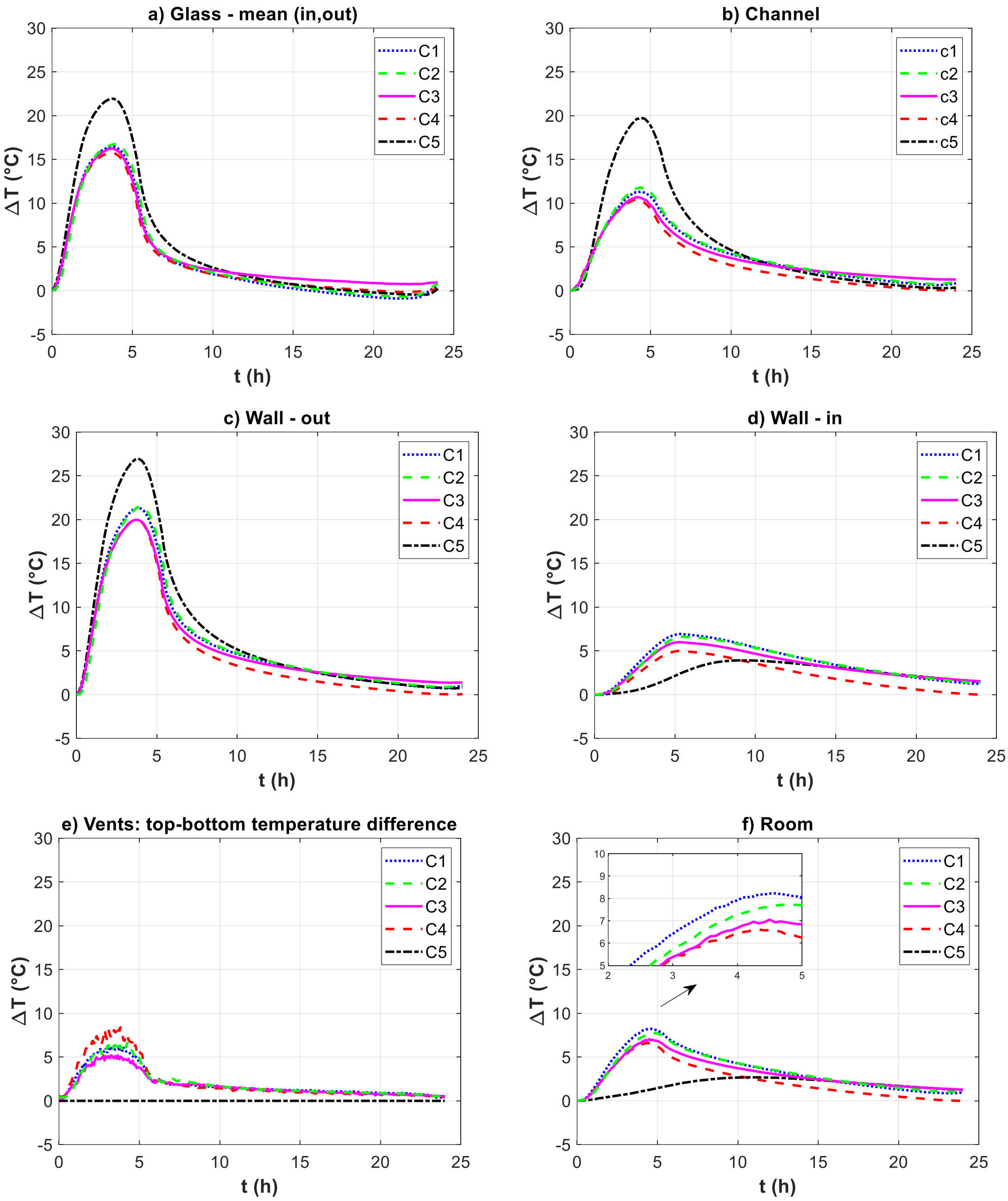

Figure 9: Influence of the vents on the mean temperature elevation

3.2.2. Stratification

If we observe the stratification in the channel (Figure 10), for all configurations with open vents (C1 to C4, Figure 10 a to d), we observe a similar stratification with a regular progression of the dimensionless temperature T^{+} with the height y^{+}. The configuration where the vents are completely closed (C5 Figure 10d) has a different shape with a modified temperature progression, probably due to the internal recirculation in the channel when it is closed. In the room (Figure 11), there is again a major difference between the open-vents and closed-vents configurations. Indeed, without an opening to the heated cavity, the temperature hardly rises (Figure 11e). The temperature of the configurations with the largest opening of the vents (C1 to C3, Figure 11a to Figure 11c) have similar appearances with almost equal T^+ values in the upper part of the room ($y^+ = 0.67$ et $y^+ = 1$). For the C4 configuration, on the other hand, the temperature progression is more regular, probably due to the lower air circulation. The wall temperature on the North wall of the room (Figure 12), again presents a major difference when the vents are closed (C5 Figure 12e). When the vents are open, there is little difference between the configurations. It can be seen that the temperature T^+ at the top of the wall at $y^+ = 1$ is lower, probably due to the thermal bridge present at this location. The C4 configuration is only distinguished by its lower temperature ranges due to the small size of the vents. This result is different from Warrington and Ameel work [36] , but in their case, liquid was used, therefore the Rayleigh number was higher.

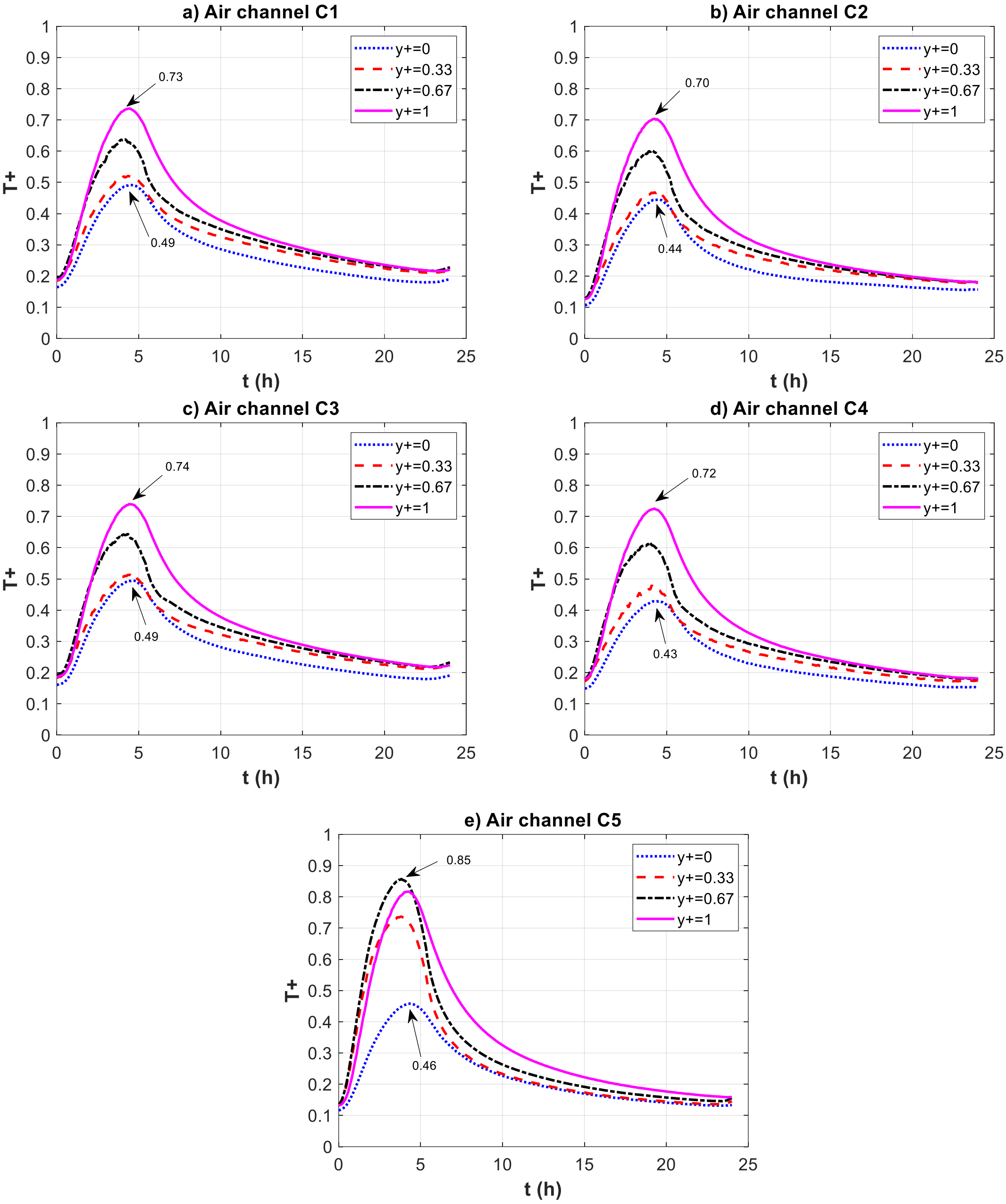

Figure 10: Influence of the vents on the stratification in the air channel

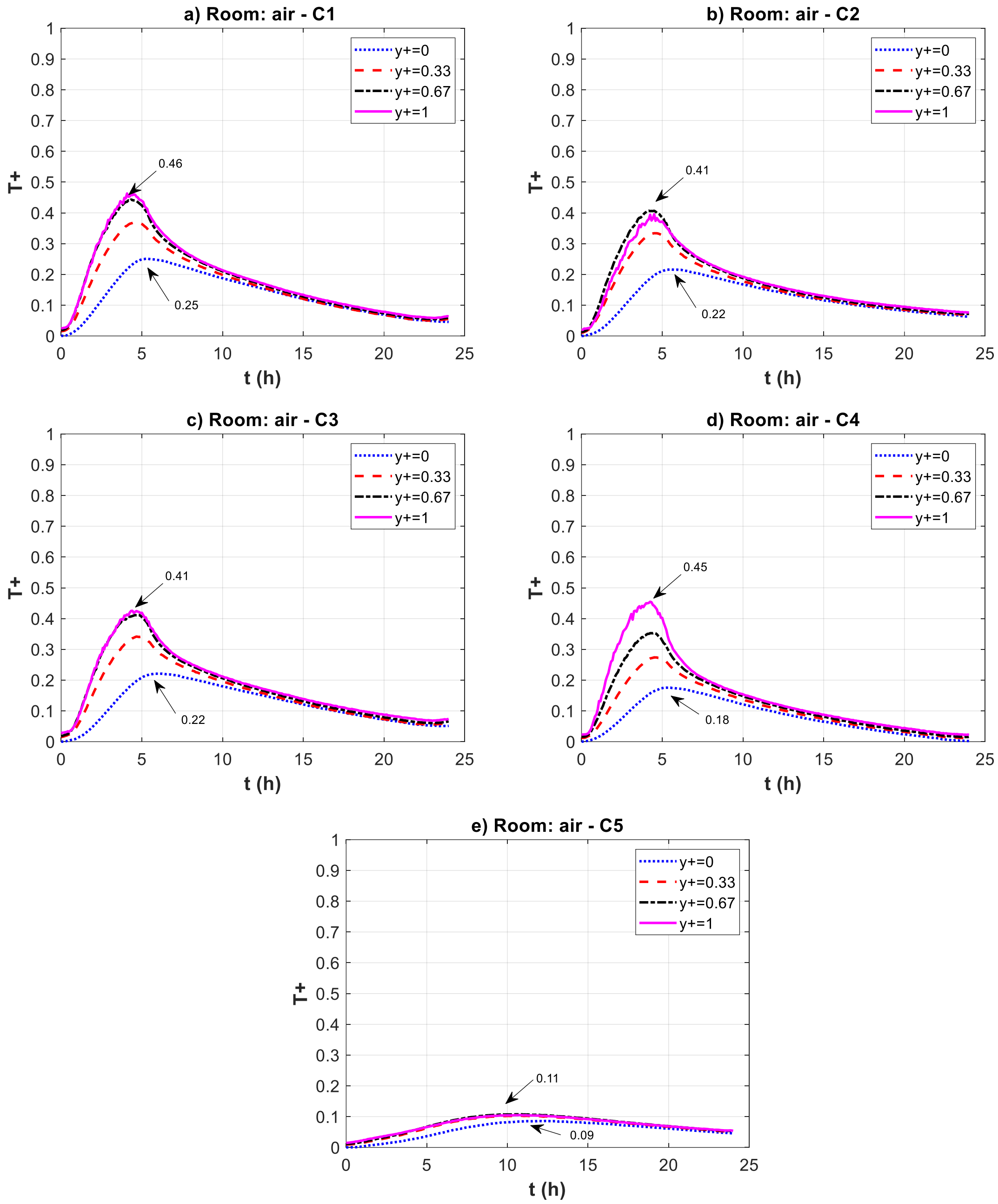

Figure 11: Influence of the vents on the stratification in the air room

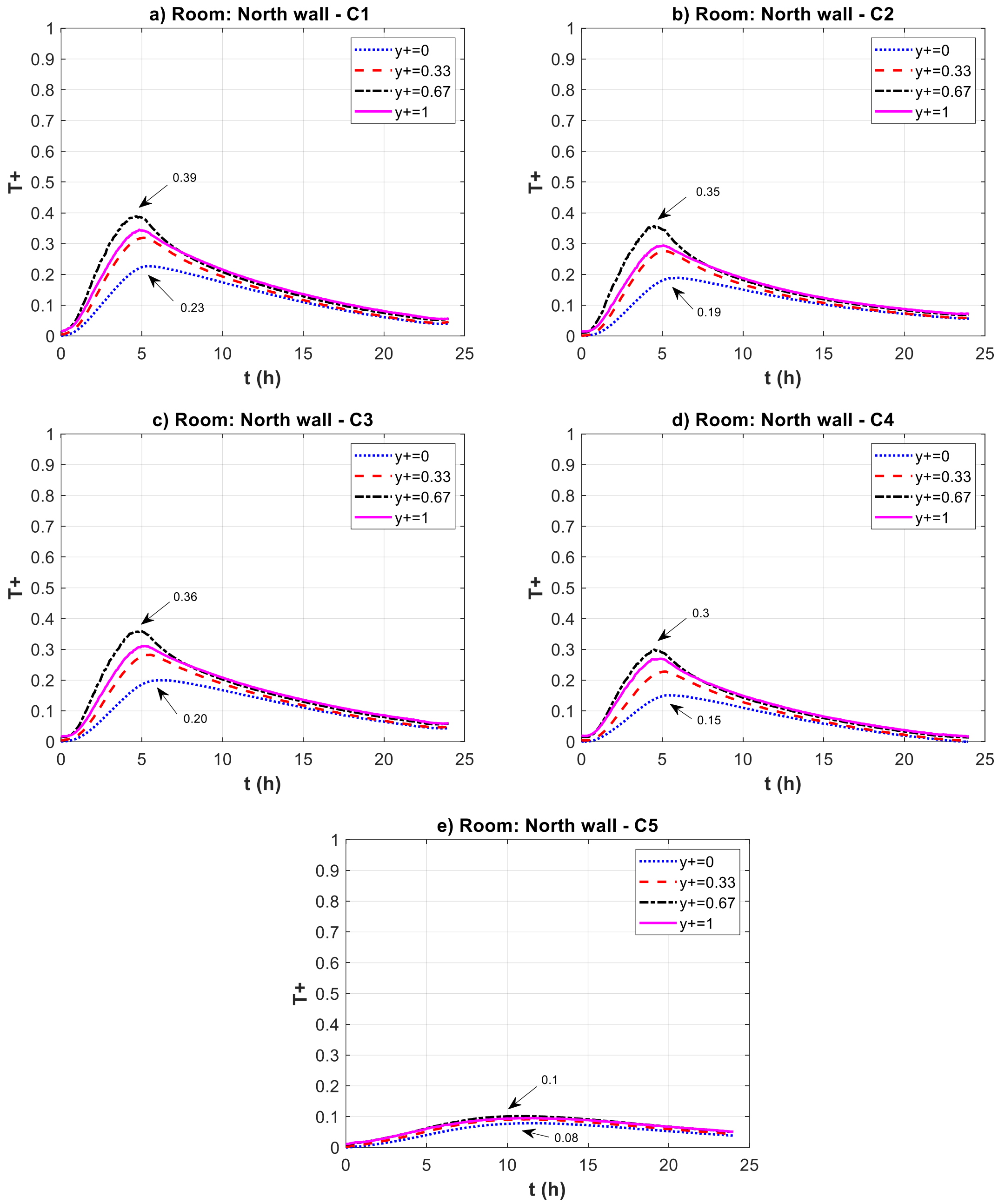

Figure 12: Influence of the vents on the stratification at the North wall of the room

3.2.3. Heat Fluxes

In this paragraph, the different heat fluxes are presented. We begin by presenting the evolution of the Rayleigh number in the cavity according to the different configurations of the vents (Figure 13). The values are significantly lower with closed vents (maximum at 4.4×10^8 compared to over 6×10^8 for open vent configurations), due to the lower temperature difference between the outside wall and the air in the channel.

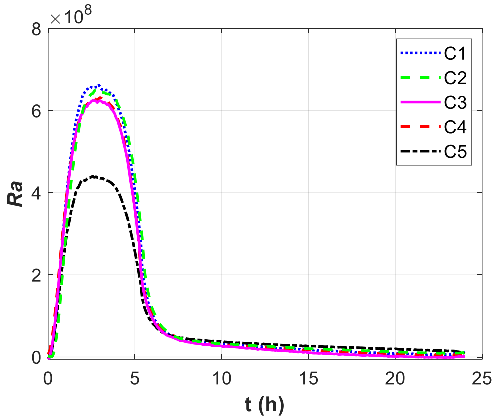

Figure 13: Rayleigh number for the different configurations

The different values of the incident heat fluxes from the light source are presented in Figure 14a. There is a maximum amplitude difference of 5% in the peak value between these different tests, which allows us to consider the conditions reproducible.

In order to present heat flux values that are more meaningful than heat transfer rate values, the convective and conductive heat transfer rate are divided by the useful surface of the Trombe wall, i.e., the surface of the glazing.

Convective heat fluxes through the vents, calculated from the heat transfer rate equation (6) and divided by the area of the glazing, are shown in Figure 14b. As the calculated heat flux depends on the passage section, the convective heat flux decreases with the section with a maximum value for the configuration C1 and a zero value for C5.

The conductive heat flux measured by the heat flux sensor is first multiplied by the wall surface and then divided by the surface of the glazing. The results are shown in Figure 14c. All configurations where the vents are open have a negative heat flux at the beginning of the day, because the cooler inside wall exchanges with the hotter air in the room (Figure 14d), as described in paragraph 3.1.1. Thus, except in the case where the vents are closed, the temperature of the room rises faster than that of the inside wall surface, thanks to the air circulation through the vents.

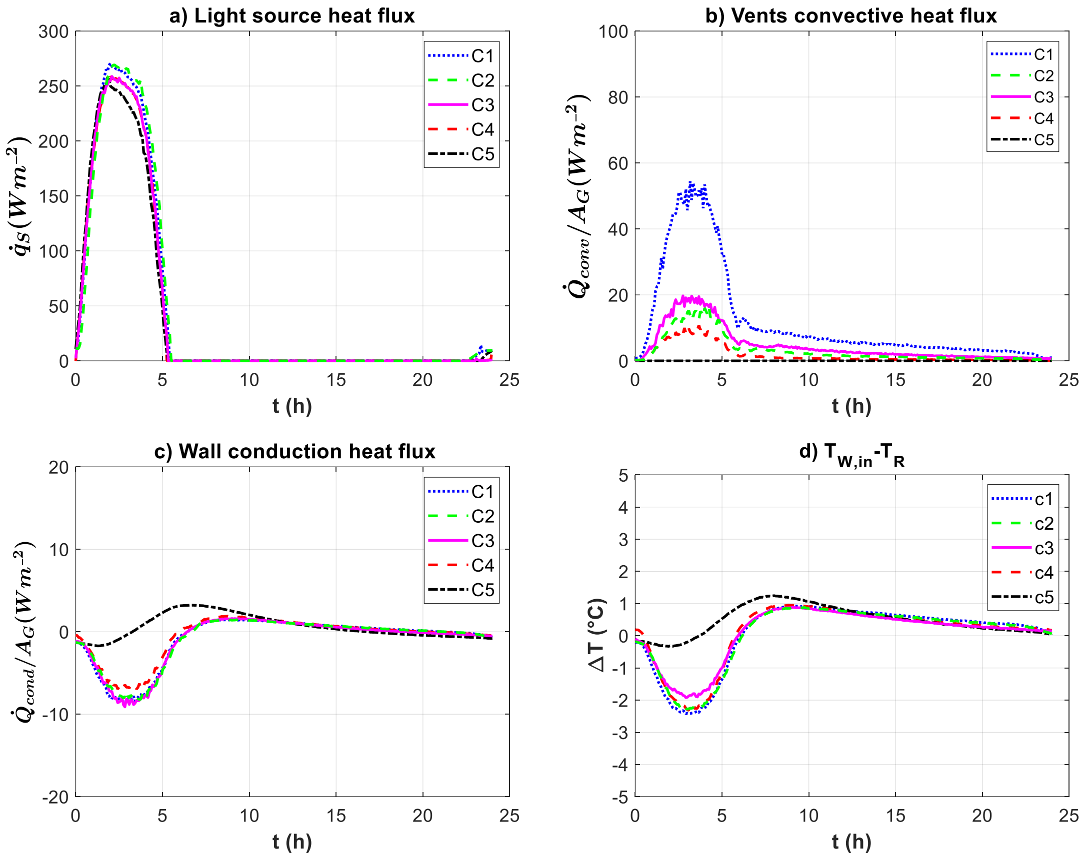

Figure 14: Influence of the vents on heat fluxes

3.2.4. Efficiencies

The influence of the shape and surface area of the vents on efficiencies is presented in Figure 15. The efficiency η_{conv} (Figure 15a) is based only on convective heat fluxes, therefore the different efficiency values vary from zero when the vents are closed to an efficiency of 28% when the cross-section is at its maximum in configuration C1. In the C2 configuration, the surface area is reduced by half, so the efficiency decreases. For the configuration C3, the cross-section is larger than that of the configuration C2, although not uniform on the wall. From a mathematical point of view, from eq. (6), the efficiency in C3 configuration will therefore be higher than that calculated in C2. However, the temperature of the room increases less in C3 than in C2 suggesting that the heat transfer is higher in the C2 configuration (Figure 9f), in contrast with the evolution of η_{conv}. It is therefore a strong limitation of the η_{conv} criterion when the velocity is not precisely known. The efficiency drops further in C4 which has the lowest cross-section.

The criterion η_{sto} (Figure 15b) shows that the configuration where the vents are closed allows for higher heat storage due to the higher temperature rise of the wall in this case. Configurations where the vents are open have lower and similar efficiencies. This criterion therefore does not make it possible to differentiate between configurations where the vents are open from one another.

The indoor temperature stability criterion, *TLL* (Figure 15c), is the lowest for the case where the vents are closed, illustrating the low heat transfer between the channel and the room in this configuration C5. On the other hand, this criterion is higher for configurations C1 and C2 which favor convective transfer and are favorable for heating the room. It is higher for C2 than C3, in accordance with the room temperature rises, even though the vents surface area is higher for C3 as discussed before. *TLL* therefore seems a meaningful criterion to analyze the configurations.

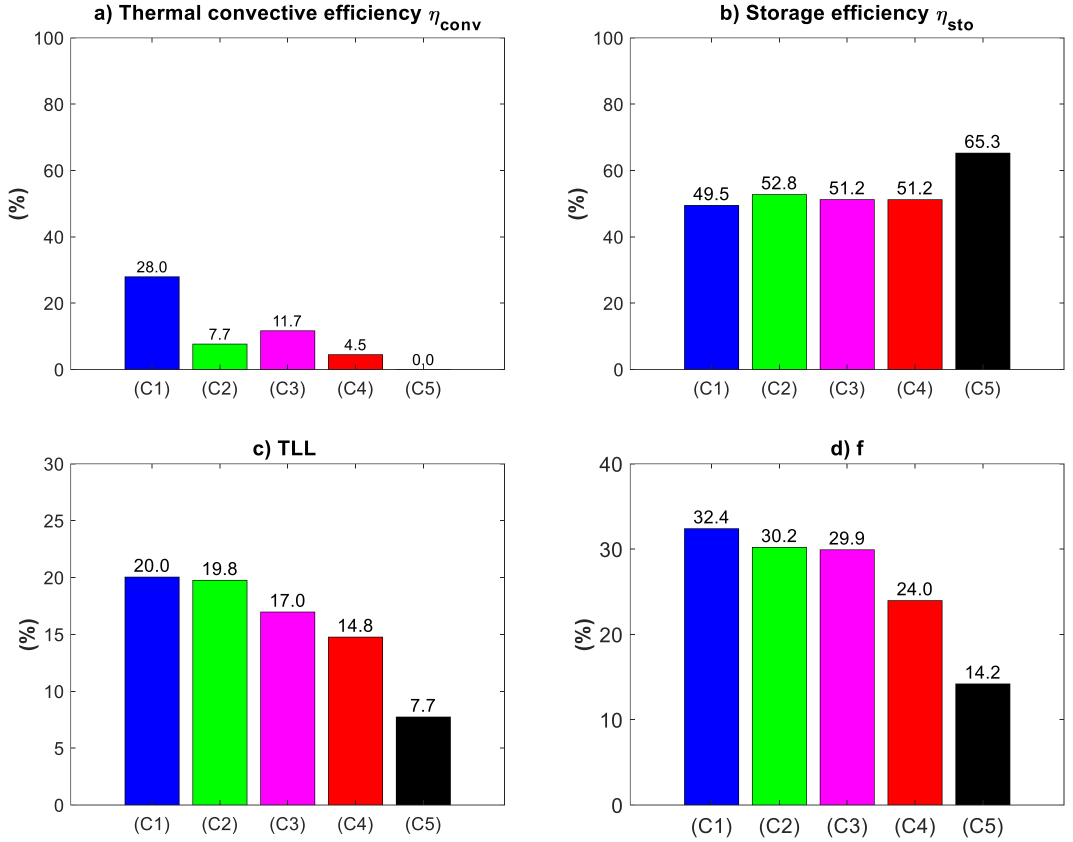

Figure 15: Influence of the vents on efficiencies.

Similarly, convective transfer tends to homogenize the temperatures in the wall and the room. Therefore, *f* is highest for the configurations where the convective transfer is the greatest, i.e. the configurations C1, followed in descending order by C2, C3, C4, and finally C5. It can be noted, however, that for the configurations C1 to C3, the value of *f* varies relatively only by 7%, which suggests a convective transfer that is ultimately slightly variable with the size of the vents. This observation was also made by Warrington and Ameel [36] in the case of a 1/18th scale model using silicone oil and for much higher values of Rayleigh number of 1.5×10^{10}. *f* seems therefore a meaningful criterion to analyze the configurations.

4. Conclusion

This article presents an experimental study of a Trombe wall made of cellular concrete, associated with specific vent configurations. The wall is connected to an adjacent room. The measurements concern the temperature and heat fluxes measured in different areas of the experiment. The conditions are those of an intermediate season. The influence of the number and configuration of the vents on thermal behavior was measured and analyzed using various criteria, and the most meaningful ones were identified. The results indicate that:

- only the configuration with the vents fully closed demonstrates significantly different thermal behavior compared to the other configurations,
- with vents fully closed, and thanks to the insulating properties of cellular concrete, the temperature rise in the room is low, making it possible to consider this solution to ensure the comfort of the inhabitants even in summer conditions,
- due to the insulating properties of cellular concrete, heat transfer is mainly carried out by convection in the Trombe wall using this material,
- reducing the size of the vents leads to a decrease in temperature rise in the adjacent room, enhances its thermal stability, and increases the temperature difference between the inside and outside of the wall,
- however, this effect remains moderate unless there is a substantial reduction in vent area, around 60%,
- therefore, to effectively limit convective transfer through partial vent closure, a significant reduction in surface area is necessary.

In general, it can be concluded that cellular concrete Trombe walls have the potential to provide passive heating and summer thermal comfort to buildings with an appropriate vent management.

Future work will focus on developing velocity measurements using Particle Image Velocimetry (PIV) and creating a CFD model to evaluate optimal vent control strategies based on varying environmental conditions.

5. References

[1] « Energy efficiency: new EU rules for buildings and homes ». [En ligne]. Disponible sur: https://www.europarl.europa.eu/news/en/headlines/economy/20180328STO00750/energy-efficiency-new-eu-rules-for-buildings-and-homes

[2] O. Saadatian, K. Sopian, C. H. Lim, N. Asim, et M. Y. Sulaiman, « Trombe walls: A review of opportunities and challenges in research and development », *Renewable and Sustainable Energy Reviews*, vol. 16, nº 8, p. 6340-6351, 2012, doi: https://doi.org/10.1016/j.rser.2012.06.032.

[3] S. Kostikov, C. Shen, et Y. Jiang, « A review of the current work potential of a trombe wall », *Renewable and Sustainable Energy Reviews*, vol. 130, p. 109947, 2020, doi: https://doi.org/10.1016/j.rser.2020.109947.

[4] E. S. Morse, « Warming and ventilating apartments by the sun's rays ». Google Patents, 6 septembre 1881.

[5] D. Wang *et al.*, « Classification, experimental assessment, modeling methods and evaluation metrics of Trombe walls », *Renewable and Sustainable Energy Reviews*, vol. 124, p. 109772, mai 2020, doi: 10.1016/j.rser.2020.109772.

[6] S. Jaber et S. Ajib, « Optimum design of Trombe wall system in mediterranean region », *Solar Energy*, vol. 85, nº 9, p. 1891-1898, 2011, doi: https://doi.org/10.1016/j.solener.2011.04.025.

[7] E. Krüger, E. Suzuki, et A. Matoski, « Evaluation of a Trombe wall system in a subtropical location », *Energy and Buildings*, vol. 66, p. 364-372, 2013, doi: https://doi.org/10.1016/j.enbuild.2013.07.035.

[8] A. Abdeen, A. A. Serageldin, M. G. E. Ibrahim, A. El-Zafarany, S. Ookawara, et R. Murata, « Experimental, analytical, and numerical investigation into the feasibility of integrating a passive

Trombe wall into a single room », *Applied Thermal Engineering*, vol. 154, p. 751-768, 2019, doi: https://doi.org/10.1016/j.applthermaleng.2019.03.090.

[9] F. Abbassi, N. Dimassi, et L. Dehmani, « Energetic study of a Trombe wall system under different Tunisian building configurations », *Energy and Buildings*, vol. 80, p. 302-308, 2014, doi: https://doi.org/10.1016/j.enbuild.2014.05.036.

[10] F. Stazi, A. Mastrucci, et C. di Perna, « The behaviour of solar walls in residential buildings with different insulation levels: An experimental and numerical study », *Energy and Buildings*, vol. 47, p. 217-229, 2012, doi: https://doi.org/10.1016/j.enbuild.2011.11.039.

[11] B. K. Koyunbaba et Z. Yilmaz, « The comparison of Trombe wall systems with single glass, double glass and PV panels », *Renewable Energy*, vol. 45, p. 111-118, 2012, doi: https://doi.org/10.1016/j.renene.2012.02.026.

[12] K. Irshad, K. Habib, et N. Thirumalaiswamy, « Energy and Cost Analysis of Photo Voltaic Trombe Wall System in Tropical Climate », *Energy Procedia*, vol. 50, p. 71-78, 2014, doi: https://doi.org/10.1016/j.egypro.2014.06.009.

[13] I. Hernandez-Lopez, J. Xaman, Y. Chavez, I. Hernandez-Pérez, et R. Alvarado-Juarez, « Thermal energy storage and losses in a room-Trombe wall system located in Mexico », *Energy*, vol. 109, p. 512-524, 2016, doi: https://doi.org/10.1016/j.energy.2016.04.122.

[14] W. He, Z. Hu, B. Luo, X. Hong, W. Sun, et J. Ji, « The thermal behavior of Trombe wall system with venetian blind: An experimental and numerical study », *Energy and Buildings*, vol. 104, p. 395-404, 2015, doi: https://doi.org/10.1016/j.enbuild.2015.06.078.

[15] X. Hong, W. He, Z. Hu, C. Wang, et J. Ji, « Three-dimensional simulation on the thermal performance of a novel Trombe wall with venetian blind structure », *Energy and Buildings*, vol. 89, p. 32-38, 2015, doi: https://doi.org/10.1016/j.enbuild.2014.12.014.

[16] Z. Hu, W. He, X. Hong, J. Ji, et Z. Shen, « Numerical analysis on the cooling performance of a ventilated Trombe wall combined with venetian blinds in an office building », *Energy and Buildings*, vol. 126, p. 14-27, 2016, doi: https://doi.org/10.1016/j.enbuild.2016.05.016.

[17] W. He *et al.*, « Thermal and hydraulic analysis on a novel Trombe wall with venetian blind structure », *Energy and Buildings*, vol. 123, p. 50-58, 2016, doi: https://doi.org/10.1016/j.enbuild.2016.04.042.

[18] X. Hong, M. K. H. Leung, et W. He, « Thermal behaviour of Trombe wall with venetian blind in summer and transition seasons », *Energy Procedia*, vol. 158, p. 1059-1064, 2019, doi: https://doi.org/10.1016/j.egypro.2019.01.257.

[19] X. Hong, M. K. H. Leung, et W. He, « Effective use of venetian blind in Trombe wall for solar space conditioning control », *Applied Energy*, vol. 250, p. 452-460, 2019, doi: https://doi.org/10.1016/j.apenergy.2019.04.128.

[20] T. G. Ozbalta et S. Kartal, « Heat gain through Trombe wall using solar energy in a cold region of Turkey », *Scientific Research and Essays*, vol. 5, nº 18, p. 2768-2778, 2010.

[21] F. Stazi, A. Mastrucci, et P. Munafò, « Life cycle assessment approach for the optimization of sustainable building envelopes: An application on solar wall systems », *Building and Environment*, vol. 58, p. 278-288, 2012, doi: https://doi.org/10.1016/j.buildenv.2012.08.003.

[22] A. C. Briga Sá, A. Martins, J. Boaventura-Cunha, J. Carlos Lanzinha, et A. Paiva, « An analytical approach to assess the influence of the massive wall material, thickness and ventilation system on the Trombe wall thermal performance », *Journal of Building Physics*, vol. 41, nº 5, p. 445-468, 2018.

[23] I. Hernandez-Lopez, E. Vazquez-Beltran, J. Xaman, Y. Chavez, J. F. Hinojosa, et F. Noh-Pat, « Heating potential prediction of a trombe wall system under temperate climate conditions of Mexico: Case of Cwa-Cwb Köppen classification », *Journal of Building Engineering*, vol. 44, p. 103308, 2021, doi: https://doi.org/10.1016/j.jobe.2021.103308.

[24] J. Dong, Z. Chen, L. Zhang, Y. Cheng, S. Sun, et J. Jie, « Experimental investigation on the heating performance of a novel designed trombe wall », *Energy*, vol. 168, p. 728-736, 2019, doi: https://doi.org/10.1016/j.energy.2018.11.125.

[25] R. Warrington et T. Ameel, « Experimental studies of natural convection in partitioned enclosures with a Trombe wall geometry », *Journal of Solar Energy Engineering*, vol. 117, nº 1, 1995.

[26] R. B. Yedder, Z.-G. Du, et E. Bilgen, « Numerical study of laminar natural convection in composite trombe wall systems », *Solar & Wind Technology*, vol. 7, nº 6, p. 675-683, 1990, doi: https://doi.org/10.1016/0741-983X(90)90042-Z.

[27] I. Kurtbas et A. Durmus, « Unsteady heat transfer by natural convection in the cavity of a passive heating room », *International Journal of Thermal Sciences*, vol. 47, nº 8, p. 1026-1042, 2008, doi: https://doi.org/10.1016/j.ijthermalsci.2007.08.001.

[28] Y. Liu, D. Wang, C. Ma, et J. Liu, « A numerical and experimental analysis of the air vent management and heat storage characteristics of a trombe wall », *Solar Energy*, vol. 91, p. 1-10, 2013, doi: https://doi.org/10.1016/j.solener.2013.01.016.

[29] N. Ghrab-Morcos, C. Bouden, et R. Franchisseur, « Overheating caused by passive solar elements in Tunis. Effectiveness of some ways to prevent it », *Renewable Energy*, vol. 3, nº 6, p. 801-811, 1993, doi: https://doi.org/10.1016/0960-1481(93)90088-X.

[30] G. Gan, « A parametric study of Trombe walls for passive cooling of buildings », *Energy and buildings*, vol. 27, nº 1, p. 37-43, 1998.

[31] L. Zalewski, M. Chantant, S. Lassue, et B. Duthoit, « Experimental thermal study of a solar wall of composite type », *Energy and Buildings*, vol. 25, nº 1, p. 7-18, 1997.

[32] P. Torcellini et S. Pless, « Trombe walls in low-energy buildings: practical experiences », National Renewable Energy Lab., Golden, CO (US), 2004.

[33] F. Stazi, A. Mastrucci, et C. di Perna, « Trombe wall management in summer conditions: An experimental study », *Solar Energy*, vol. 86, p. 2839-2851, 2012.

[34] N. Simões, M. Manaia, et I. Simões, « Energy performance of solar and Trombe walls in Mediterranean climates », *Energy*, vol. 234, p. 121197, 2021, doi: https://doi.org/10.1016/j.energy.2021.121197.

[35] P. Bevilacqua, R. Bruno, J. Szyszka, D. Cirone, et A. Rollo, « Summer and winter performance of an innovative concept of Trombe wall for residential buildings », *Energy*, vol. 258, p. 124798, 2022, doi: https://doi.org/10.1016/j.energy.2022.124798.

[36] R. Warrington et T. Ameel, « Experimental studies of natural convection in partitioned enclosures with a Trombe wall geometry », 1995.

[37] A. de Gracia, L. Navarro, A. Castell, Á. Ruiz-Pardo, S. Alvárez, et L. F. Cabeza, « Experimental study of a ventilated facade with PCM during winter period », *Energy and Buildings*, vol. 58, p. 324-332, 2013, doi: https://doi.org/10.1016/j.enbuild.2012.10.026.

[38] S. Corasaniti, L. Manni, F. Russo, et F. Gori, « Numerical simulation of modified Trombe-Michel Walls with exergy and energy analysis », *International Communications in Heat and Mass Transfer*, vol. 88, p. 269-276, 2017, doi: https://doi.org/10.1016/j.icheatmasstransfer.2017.09.005.

[39] D. Wang *et al.*, « Classification, experimental assessment, modeling methods and evaluation metrics of Trombe walls », *Renewable and Sustainable Energy Reviews*, vol. 124, p. 109772, 2020, doi: https://doi.org/10.1016/j.rser.2020.109772.

[40] J. Shen, S. Lassue, L. Zalewski, et D. Huang, « Numerical study on thermal behavior of classical or composite Trombe solar walls », *Energy and Buildings*, vol. 39, nº 8, p. 962-974, 2007, doi: https://doi.org/10.1016/j.enbuild.2006.11.003.

[41] M. Rabani et M. Rabani, « Heating performance enhancement of a new design trombe wall using rectangular thermal fin arrays: An experimental approach », *Journal of Energy Storage*, vol. 24, p. 100796, 2019, doi: https://doi.org/10.1016/j.est.2019.100796.

[42] F. Taffesse, A. Verma, S. Singh, et G. N. Tiwari, « Periodic modeling of semi-transparent photovoltaic thermal-trombe wall (SPVT-TW) », *Solar Energy*, vol. 135, p. 265-273, 2016, doi: https://doi.org/10.1016/j.solener.2016.05.044.

Acknowledgements

This work has been supported by the EIPHI Graduate School (contract ANR-17-EURE-0002) and the Region Bourgogne-Franche-Comté.